Materials Research Bulletin 47 (2012) 1500–1507

Contents lists available at SciVerse ScienceDirect

Materials Research Bulletin

journal homepage: www.elsevier.com/locate/matresbu

Preparation of magnetic photocatalyst nanoparticles—TiO_2/SiO_2/Mn–Zn ferrite—and its photocatalytic activity influenced by silica interlayer

Kritapas Laohhasurayotin *, Sudarat Pookboonmee, Duangkamon Viboonratanasri, Wiyong Kangwansupamonkon

National Nanotechnology Center (NANOTEC), National Science and Technology Development Agency (NSTDA), 111 Thailand Science Park, Phahonyothin Rd., Klong 1, Klong Luang, Patumthani 12120, Thailand

ARTICLE INFO

Article history:
Received 1 August 2011
Received in revised form 29 December 2011
Accepted 19 February 2012
Available online 5 March 2012

Keywords:
A. Magnetic materials
B. Chemical synthesis
C. Electron microscopy
D. Catalytic properties
D. Magnetic properties

ABSTRACT

A magnetic photocatalyst, TiO_2/SiO_2/Mn–Zn ferrite, was prepared by stepwise synthesis involving the co-precipitation of Mn–Zn ferrite as a magnetic core, followed by a coating of silica as the interlayer, and titania as the top layer. The particle size and distribution of magnetic nanoparticles were found to depend on the addition rate of reagent and dispersing rate of reaction. The X-ray diffractometer and transmission electron microscope were used to examine the crystal structures and the morphologies of the prepared composites. Vibrating sample magnetometer was also used to reveal their superparamagnetic property. The UV–Vis spectrophotometer was employed to monitor the decomposition of methylene blue in the photocatalytic efficient study. It was found that at least a minimum thickness of the silica interlayer around 20 nm was necessary for the inhibition of electron transference initiated by TiO_2 and Mn–Zn ferrite.

1. Introduction

Metal oxides have attracted a lot of attention in recent decades due to their advantages in many applications [1]. Some metal oxides such as TiO_2, ZnO, and V_2O_5 are generally known to possess a photocatalytic capability that can be used to eliminate substances including both organic and inorganic chemicals. Once irradiated, the photocatalyst generates excited electrons and positive holes that further react with O_2 and H_2O to form the superoxide anion (O_2^-) and hydroxyl radical ($OH^\bullet$), respectively [2]. These two species possess strong oxidizing capability [3]. The annihilation activity is so efficient that even the supporting material in which the particular photocatalyst has been incorporated may also deteriorate, causing a decline in application lifetime. Due to this problem, free forming TiO_2 nanoparticles may be a better choice for use since there should be no such self-degrading problem in the pure form of that photocatalyst application. However, since the TiO_2 nanoparticle is very small, its use as a suspension or in colloid form is not practical, and it may raise some environmental concerns.

The incorporation of two different materials to acquire two functions and probably achieve synergy, formulating the third additional property, has been suggested in several areas of research [4–6]. Ferrites (Fe_3O_4) and their substituted forms such as $NiFe_2O_4$, $MnFe_2O_4$, $CoFe_2O_4$, etc., are known as magnetic materials in which the crystal lattice arrangement offers the inducible magnetic domains by the external magnetic field [7]. The TiO_2 nanoparticles that are assembled with the magnetic materials mentioned above can be used for water treatment in such a way that the as-formed composite is applied photo-catalytically and recovered simply by a strong magnetic source.

Recently, many research groups have reported preparations of magnetic photocatalyst nanoparticles [8–12]. Photocatalytic capability observed with a magnetic property is considered to be useful for waste water remediation. However, thorough investigation regarding the synergistic functions resulting from the composite magnetism and photocatalysis are not well established; for example, the altered physicochemical properties caused by the electronic interaction between ferrite and the TiO_2 layer as they connect to each other as in the form of two semiconductors [13]. The electron transferring from one metal oxide to the other leads to interference in both phases, partially changing their electronic structures, and thus they cannot maintain their original properties. As a result, in the case of the magnetic photocatalyst, the dissolution of the magnetic core and a decline in photocatalytic efficacy has been observed [14]. The presence of an amorphous medium like silica or alumina, as a fence inhibiting electron transferring between the TiO_2 and magnetic phases, has been introduced to prevent such drawbacks [15–19].

* Corresponding author. Tel.: +662 564 7100x6628; fax: +662 564 6981.
E-mail address: kritapas@nanotec.or.th (K. Laohhasurayotin).

0025-5408/$ – see front matter © 2012 Elsevier Ltd. All rights reserved.
doi:10.1016/j.materresbull.2012.02.030

Mn–Zn ferrite is commonly known for its outstanding magnetic property with high magnetic polarizability and electric resistance, which has led to its widespread use in numerous electronic and magnetic applications [7]. The synthesis of titania-coated Mn–Zn ferrite nanoparticles from $TiCl_4$ was carried out earlier by Ma et al. [20], but since the electron inhibitory effect provided by amorphous silica had not been used, the photocatalytic result was not that successful. In fact, the magnetism of the composite was reported to be ferromagnetic. This, therefore, opens up the chance of permanent aggregation in the photocatalyst, which may make it ineffective for use in water purification.

We report herein the preparation of a magnetically separable photocatalyst, $TiO_2/SiO_2/Mn_{0.5}Zn_{0.5}Fe_2O_4$ from stepwise synthesis started with the co-precipitation from Mn^{2+}, Zn^{2+}, and Fe^{2+} ions, followed by hydrolyses of SiO_2 and TiO_2 precursors. The core–shell composites were characterized by several techniques including TEM, SEM, and XRD. The photocatalytic activity was examined using a spectroscopic method. In addition, we studied the effect of silica thickness on the as-prepared photocatalysts upon photocatalytic efficiency, and it was found that the missing silica interlayer led to the complete suppression of photocatalytic activity. It can be suggested that at least a minimum of about a 20 nm silica layer must be provided to avoid the electronic interaction between the two semiconductors.

2. Experimentation

2.1. Materials

All chemical reagents were of analytical grade and used without further purification. $MnSO_4{\cdot}H_2O$ and ammonium hydroxide (30%) were purchased from Carlo Erba, $FeSO_4{\cdot}7H_2O$ was purchased from Fischer, and $ZnSO_4{\cdot}7H_2O$ was purchased from Rankem. Tetraethyl orthosilicate (TEOS) and titanium (IV) tert-butoxide were purchased from Fluka. Methylene blue ($C_{16}H_{18}N_3ClS{\cdot}2H_2O$) was purchased from Unilab, and absolute ethanol and acetone were purchased from Merck.

2.2. Preparation of Mn–Zn ferrite nanoparticles (MZF)

A 30 mL mixed solution of Mn^{2+}, Zn^{2+}, and Fe^{2+} was prepared from 10 mL each of aqueous 0.057 M $MnSO_4{\cdot}H_2O$, 0.057 M $ZnSO_4{\cdot}7H_2O$, and 0.23 M $FeSO_4{\cdot}7H_2O$, respectively, in a 100 mL round bottom flask. These stoichiometric proportions led to the formation of atomic ratios 1:1:4 for Mn:Zn:Fe in $Mn_{0.5}Zn_{0.5}Fe_2O_4$. While stirring vigorously, 1.78 M NH_4OH was added to the metal solution giving a dark green precipitate of metal hydroxide. This dispersion phase was carried out in three different ways, by (1) magnetic stirrer; (2) homogenizer; and (3) mechanical stirrer. The reaction flask was then placed in an oil bath and heated up to 90–100 °C for 1 h. 20 mL DI water was added to the resulting mixture and the brown precipitate was separated by centrifugation. The precipitate was washed with several cycles of water and acetone. After separation, the brown precipitate was gradually cooled to room temperature.

2.3. Preparation of SiO_2/Mn–Zn Ferrite (S-MZF)

The typical method for the coating of SiO_2 on the MZF surface was done according to the following procedure: An amount of MZF (180 mg) was placed in a 100 mL round bottom flask containing a 1:5 mixed solution of water and ethanol (30 mL). This mixture was dispersed by an ultrasonicator for a few minutes and placed in a sonicator bath. TEOS (30 μL) and 30% NH_4OH (40 μL) were then added and the hydrolysis was allowed to proceed for 10 min before additional amounts of TEOS and NH_4OH were added. This addition step was carried out until the total volume of TEOS reached 450 μL and the reaction mixture was further dispersed in a sonicator bath at room temperature for 45 min. The resulting mixture was washed with water and ethanol using centrifugation and the collected precipitate was dried at room temperature.

2.4. Preparation of TiO_2/SiO_2/Mn–Zn ferrite (TS-MZF) and TiO_2/Mn–Zn ferrite (T-MZF)

The coating of TiO_2 on the S-MZF or MZF surface was done according to the following procedure: An amount of S-MZF or MZF (150 mg) in a round bottom flask was dispersed in a 1:14 mixed solution of water and ethanol (75 mL) in a sonicator for 20 min. Titanium (IV) tert-butoxide (0.5 mL) in ethanol (10 mL) was added to this solution mixture and the resulting mixture was stirred in an oil bath at room temperature, heated up to 90 °C and further maintained at this temperature for 2 h. A condenser was used to prevent the vaporization of the solvent. The resulting particles were separated using centrifugation and washed with several cycles of water and ethanol. Composite particles were dried in an oven at 60 °C for 24 h and calcined at 500 °C for 2 h.

2.5. Photocatalytic activity

An amount of catalysts (10 mg MZF, T-MZF, TS-MZF) was dispersed in 25 mL of 3 ppm methylene blue (MB) aqueous solution. Since energy dispersive analysis indicated that 10% of the TiO_2 was incorporated on the composite, 1 mg of pure TiO_2 was used in the comparative study. The adsorption/desorption of MB molecules on the catalyst surface was allowed until saturation for 18 h before UV analysis. To conduct the experiment, this suspension was irradiated with 20 W low pressure Hg lamps (366 nm). Each 1.4 mL suspension at 2-min intervals from 0 to 12 min and 10-min intervals from 20 to 100 min was collected, and the precipitate was separated by centrifugation. The clear solution was transferred into a cuvette cell and subsequently analyzed by UV–Vis spectrophotometer to observe the decrease in the absorbance at 664 nm. To investigate the effect of the silica interlayer on the photo-activity of the catalyst, TS-300 (300 μL TEOS was used to form the silica coating layer) was also employed.

2.6. Recyclability of TS-MZF

To a 50 mL beaker, 10 mg of TS-300 and 25 mL of 3 ppm MB were added and stirred in the dark for 18 h. Once the TS-300 particles were collected at the bottom of the beaker by an external magnet, a suspension of MB was drawn by Pasteur pipette (1.4 mL), centrifuged to get a clear solution, and measured with a UV–Vis spectrophotometer. The monitoring period was 100 min with 20 min intervals. The used TS-300 was rinsed several times with DI water by centrifugation and dried at room temperature before the next experiment. All photocatalytic reactions were done in triplicate.

2.7. Characterization methods

Scanning electron microscopy (SEM) and energy dispersive X-ray spectroscopy (EDS) measurements of the samples were obtained from HITACHI S-3400 microscope and EMAX Horiba, respectively. The transmission electron microscopy (TEM) was recorded by JEOL JEM 2010, and average particle sizes were estimated from ten particles at 50,000× magnification. X-Ray diffraction patterns were obtained from JEOL JDX 3530. Saturated magnetization (M_s) and the hysteresis curve were recorded by Lakeshore 7404 Vibrating sample magnetometer.

3. Results and discussion

3.1. Formation of magnetic nanoparticles by co-precipitation method

The MZF nanoparticle in this report was synthesized using a chemical co-precipitation method modified from the literature [21,22]. This co-precipitation is known to involve two sequencing steps of hydrolysis and oxidation of alkaline $Fe(OH)_2$ in the presence of Mn^{2+} and Zn^{2+} ions. Based on Schikorr's reaction [23], the precipitate is formed as the inverse spinel structure [24,25]:

$$xMn^{2+} + yZn^{2+} + (3 - x - y)Fe^{2+} + 6OH^- + 1/2O_2 \rightarrow Mn_xZn_yFe_{3-x-y}O_4 + 3H_2O$$

Because of its simplicity, co-precipitation is one of the most preferable methods for the preparation of magnetic particles. However, the large polydispersity of the forming particles is not desirable. Scientists have developed some procedures in order to control the particle size [21,24,26,27]. A microemulsion method described by a Slovenian group [22] was followed by our laboratory. This method was expected to result in monodispersed magnetic particles with a diameter range under 10 nm. However, this attempt was unsuccessful due to difficulty in adjusting the reaction condition. The synthesis ended up giving non-magnetic nanoparticles as a result. The synthetic approach was changed to the simpler approach of co-precipitation reaction, which was mainly controlled by stirring rate and an addition technique that did not require stabilizers [21]. It appeared that under a properly controlled temperature, rate of base addition, and rate of stirring,

Table 1
Reaction conditions and particle sizes of Mn–Zn ferrites.

Sample	Addition	Dispersion	Vol. (mL)	Average diameter (nm)[a]
MZF1	One shot	Stirring	15	8.7 ± 2.0
MZF2	Dropwise	Stirring	15	67.5 ± 11.8
MZF3	Dropwise	Homogenizing	20	10.8 ± 1.8
MZF4	One shot	Stirring	90[b]	49.4 ± 14.2

[a] Measured and averaged from TEM.
[b] Mechanical stirrer.

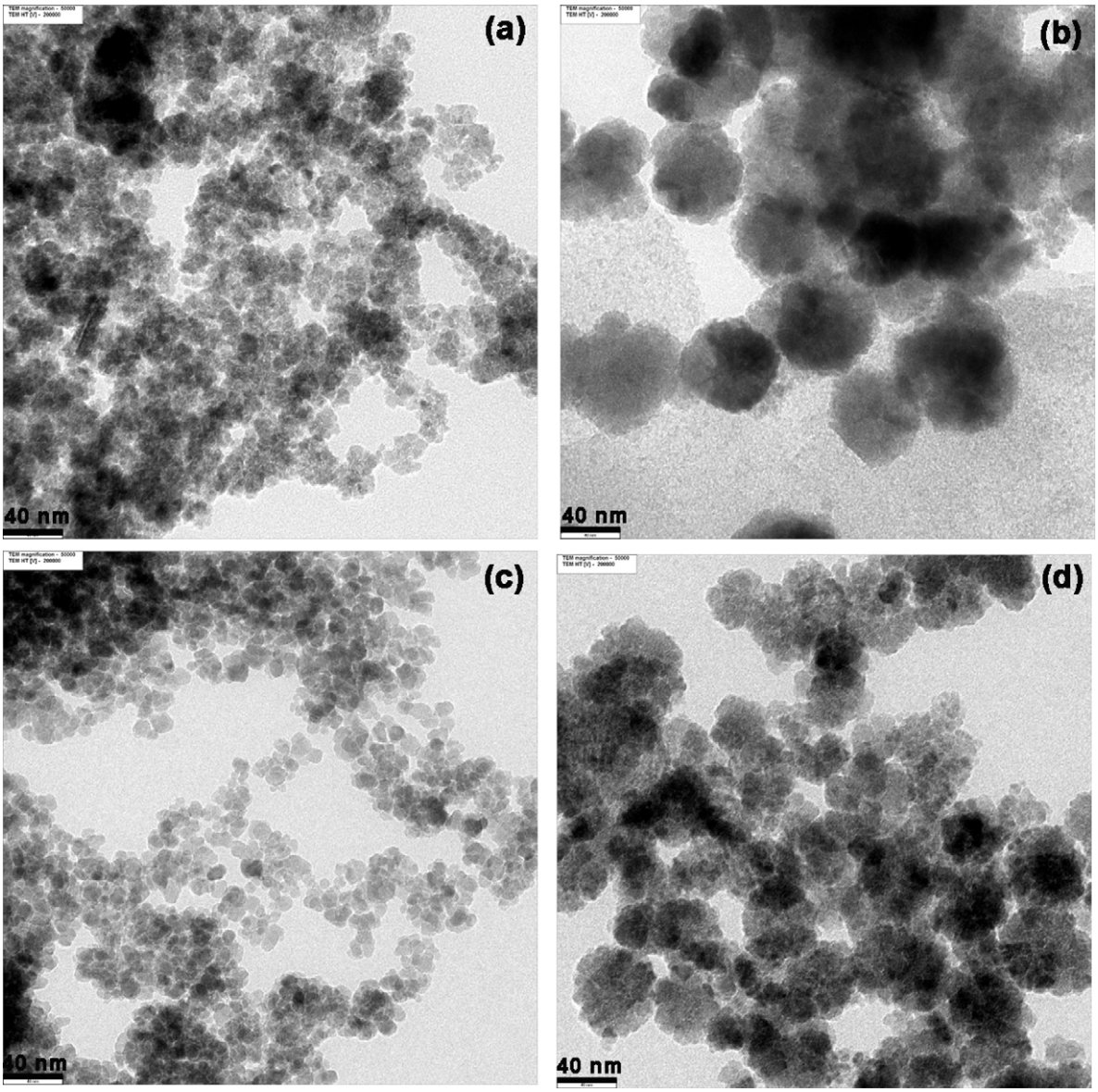

Fig. 1. TEM images of Mn–Zn ferrite: (a) MZF1, (b) MZF2, (c) MZF3, (d) MZF4.

monodispersed magnetic particles could be successfully prepared. Table 1 shows the conditions and particle sizes of the as-prepared MZFs.

The different rates of reagent addition used in the preparations of MZF1 and MZF2 led to different forming diameters of the as-obtained products. The average diameter of MZF1 was shorter than that of MZF2. This suggested that there was a difference in the initial formations of their nuclei (metal hydroxides) soon after the base addition. Originating when mixing the metal ion solutions with NH_4OH base, as in MZF1, the nuclei were formed at very same time, leading to uniform particle formation. On the other hand, the dropwise practice slowly formed a number of precipitate nuclei, and subsequently the addition of base in the same mixing course was only to be used in the growth of the already formed particles, resulting in aggregated particles. The size of the particle increased non-homogeneously and therefore became more polydispersed.

Besides the addition rate, the mixing of the reaction mixture is also crucial in the formation of size-gaining particles. This could be explained in terms of homogeneity of the reaction. By stirring the reaction rapidly to obtain a homogeneous system, the growth of each nanoparticle occurred at a similar rate, thus leading to narrow polydispersity. MZF3 was obtained by dispersion with a homogenizer, which provided narrow size dispersity (10.8 nm).

The series in Fig. 1 presents the TEM results of the prepared magnetic particles under the experimental conditions shown in Table 1. It is clearly seen that the rapid addition of NH_4OH resulted in small particles (Fig. 1a; MZF1) while the slow addition resulted in large particle aggregates (Fig. 1b; MZF2). Furthermore, the influence of homogeneity seemed to be far more important as it was found that the homogenized reaction offered narrow size dispersity with a non-aggregated characteristic in MZF3 (Fig. 1c). The morphology of MZF4 in Fig. 1d, however, indicates the significance of homogeneity in the preparation. Its particle sizes were scattered, and the aggregated forms were mainly observed. This is because when the reaction volume increased (90 mL), the homogeneity of the reaction was difficult to control.

In Fig. 2(a), the HREM image of MZF3 revealed the particle crystallinity. With electron diffraction as shown in Fig. 2(b), the crystalline MZF shows consistent evidence to the spinel ferrite structure with the interplanar distance around 0.25 nm of (3 1 1) plane [25]. This value was congruent with the 2.5 Å calculated by applying Bragg's equation [28] on the XRD result of a representative MZF. The EDS shown in Fig. 3 and the data of element atomic ratios revealed that $Mn_{0.5}Zn_{0.5}Fe_2O_4$ was genuinely formed (Mn:Zn:Fe = 1:1:4).

Fig. 4 shows the magnetization curves of MZF1, MZF3, and MZF4. The S-shape of the curves confirmed the superparamagnetism of the MZF materials. The saturation magnetization of MZF3 (M_s = 44.5 emu/g) was higher than those of the other two samples (M_s = 35.0 and 32.9 emu/g for MZF1 and MZF4, respectively). This could be due to the high uniformity of the MZF3 nanoparticles, implying that its crystallinity was well aligned. The very close saturation magnetizations of MZF2 and MZF4, though they were formed differently in shape, indicated that the reaction environments, i.e. reaction temperature, time, and pH were appropriate for producing the same magnetic quality.

3.2. Coating of silica on Mn–Zn ferrite (S-MZF)

The series in Fig. 5 presents the TEM images of the S-MZF obtained by varying the amount of TEOS in the coating step on the suspended MZF. As the reaction time was set to be the same, the only effect on the coating layer of silica was the difference in TEOS amount that led to a different thickness of silica coating. The TEM image in Fig. 5a reveals that the silica layer was not formed, although 150 μL of TEOS was used for coating. This might be due to the inadequate silica precursor that was to be formed as silica over the aggregated MZF particles. Fig. 5b and c shows that a greater amount of TEOS provided adequate silica to cover the magnetic particles as TEOS was increased from 150 μL to 300 and 450 μL, resulting in 15 and 22 nm thick silica over the MZF core. The silica coating on the magnetic particle was proposed by aiming to reduce the electronic interaction between the core magnetic Mn–Zn ferrite and the outer layer, TiO_2 [15–19]. This was done intentionally to prevent the photodissolution of the magnetic core and the declined photoactivity resulted from the two semiconductor synergistic effect [8,13,29]. It was suggested that this phenomenon involves the thermodynamic feasibility of the excited electron on a photocatalyst conduction band that was transferred into another lower conduction band of metal oxide. The resulting lower band gap from metal oxide further enhanced electron–hole recombination, thus lowering the photoactivity of the photocatalyst [9].

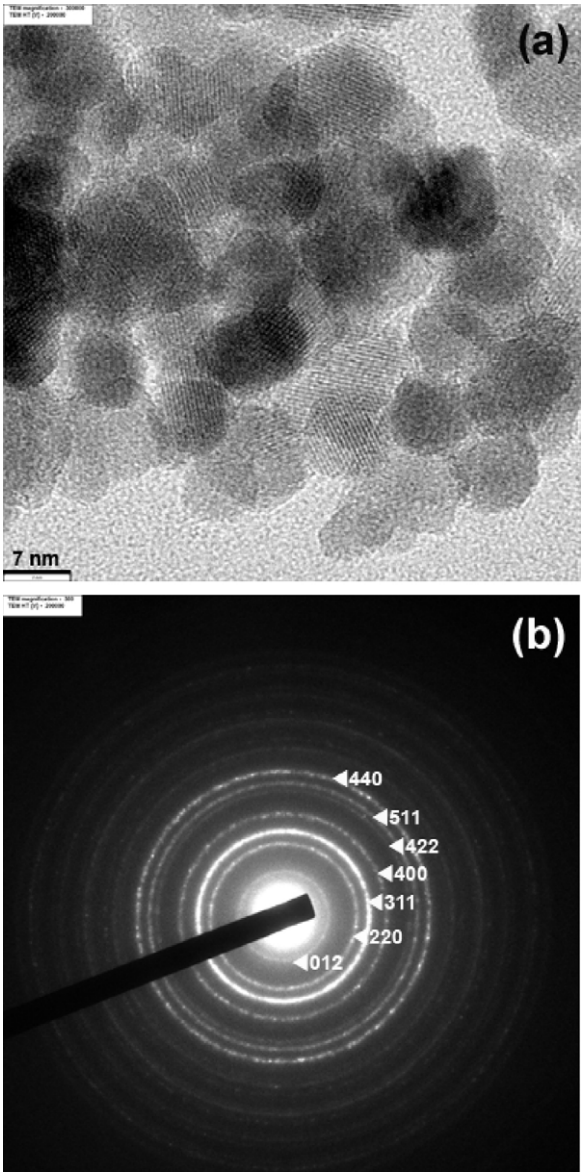

Fig. 2. (a) HREM image of MZF2 and (b) Electron diffraction of MZF2.

3.3. Coating of titanium dioxide on SiO_2/Mn–Zn ferrite (TS-MZF)

Titanium dioxide coating on S-MZF was confirmed by the TEM image shown in Fig. 6(a). It reveals the rough surface of TiO_2 on the

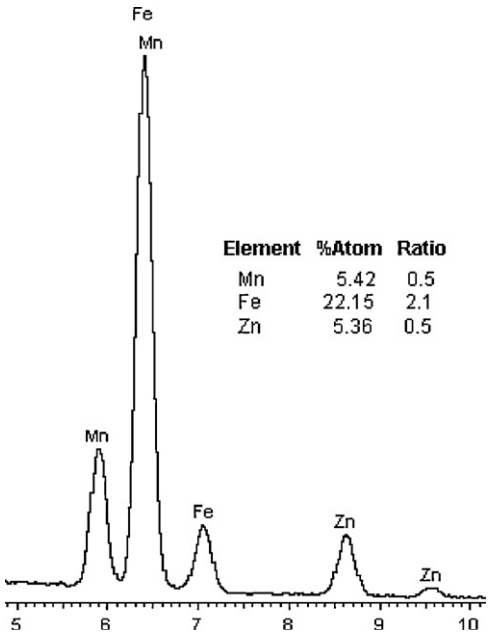

Fig. 3. EDS result of a representative $Mn_{0.5}Zn_{0.5}Fe_2O_4$ (MZF).

S-MZF particle. This roughness was obtained due to the rapid hydrolysis rate of TBOT in a basic solution, as opposed to the smooth layer of silica obtained by a slower hydrolysis rate [10]. The morphology of T-MZF (no silica interlayer) was also examined by TEM as shown in Fig. 6(b), demonstrating that not only did TiO_2 nanoparticles sinter themselves into larger particles, but they also merged their edges with the MZF core. The phase separation between the two metal oxides almost disappeared.

The XRD result of the TS-MZF is compared with those of S-MZF and pure MZF in Fig. 7. Each XRD pattern corresponded to the phase compositions truly present in the as-prepared products. The XRD patterns of MZF before and after SiO_2 coating (S-MZF) were almost the same except that a broad signal from 20 to 28° of 2θ due to amorphous silica clearly appeared in S-MZF and in TS-MZF as well. The coating TiO_2 on S-MZF was confirmed by the appearance of some peaks due to the anatase TiO_2, essentially at 25° and 47° regarding the (1 0 1) and (2 0 0) planes, respectively (JCPDS File No. 21-1272).

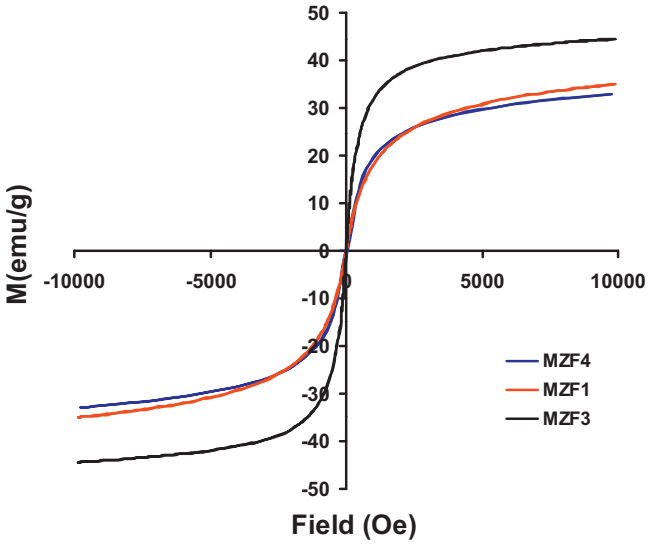

Fig. 4. Magnetization measurement of MZFs at room temperature.

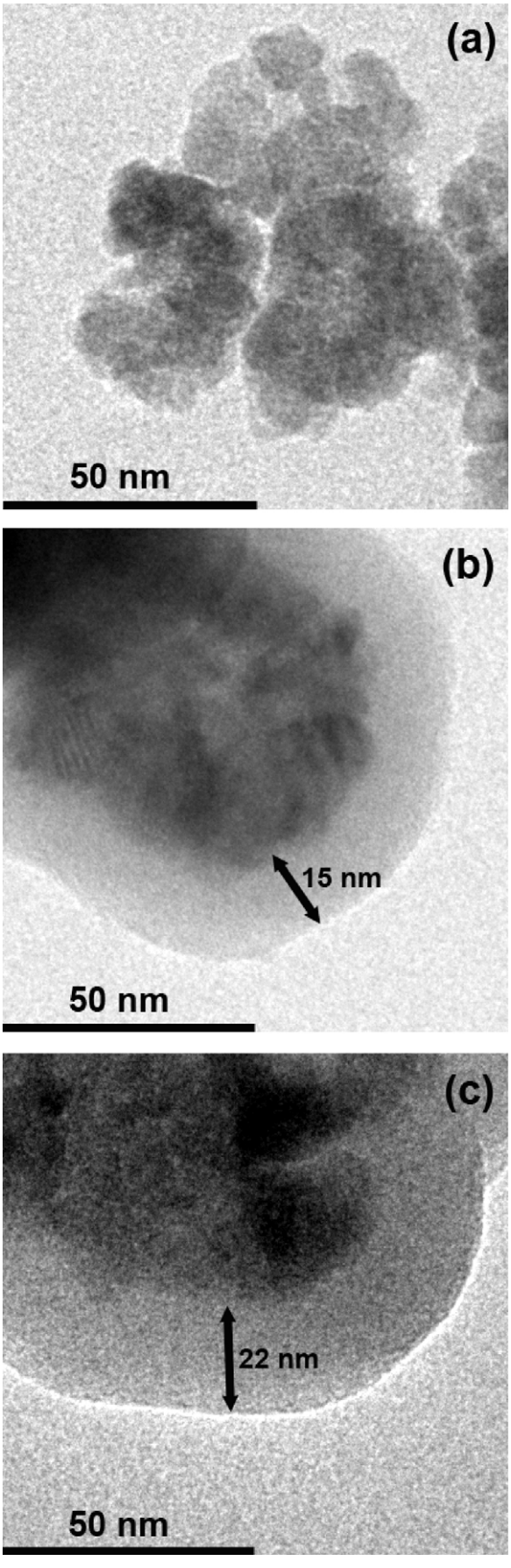

Fig. 5. TEM images of S-MZF prepared from: (a) 150 μL, (b) 300 μL, and (c) 450 μL TEOS.

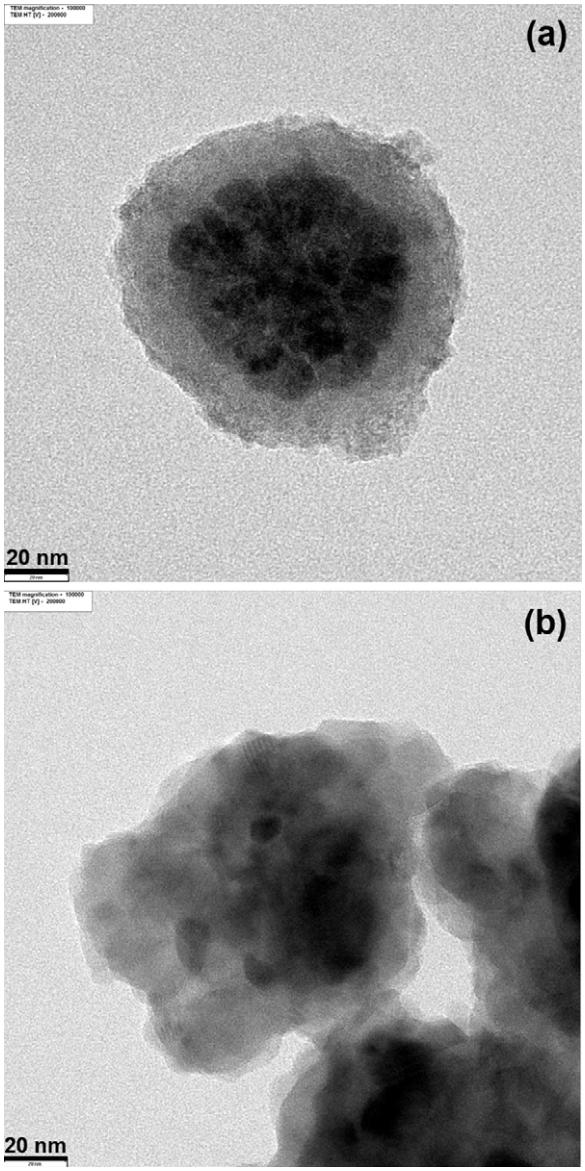

Fig. 6. TEM images of (a) TS-MZF and (b) T-MZF.

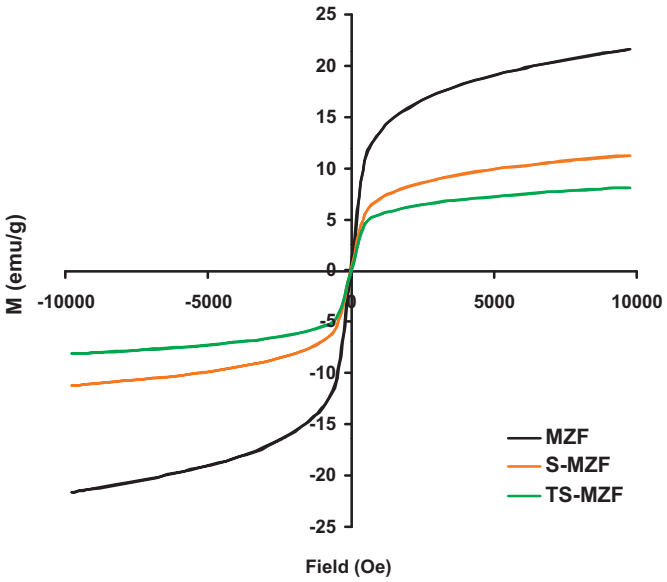

Fig. 8. Magnetization measurement of representative MZF, S-MZF, and TS-MZF.

Fig. 8 shows the magnetic property of TS-MZF compared with MZF and S-MZF. The decreases in saturating magnetization from that of the original MZF were observed after two coatings from 20 to 10 and 8 emu/g for MZF, S-MZF, and TS-MZF, respectively. This could have resulted from the non-magnetic volume, which increased with the additional layers of TiO_2 and SiO_2 [30]. It is worth noting that the silica coating step caused a greater decrease in magnetization than the titania coating step did. This is probably because of the thicker silica layer compared to the TiO_2 layer.

3.4. Photocatalytic activity

Fig. 9 shows the photodecomposition of methylene blue upon UV irradiation in the presence of the selected catalysts. Of the five samples, three samples, TS-MZF, TS-300 and pure TiO_2, exhibited photocatalytic performance during 100 min of irradiation. More than 90% MB was decomposed by TiO_2, whereas nearly 80% MB was decomposed by TS-MZF. Less than 40% MB decomposition was observed in the case of TS-300. Interestingly, the trends of MB

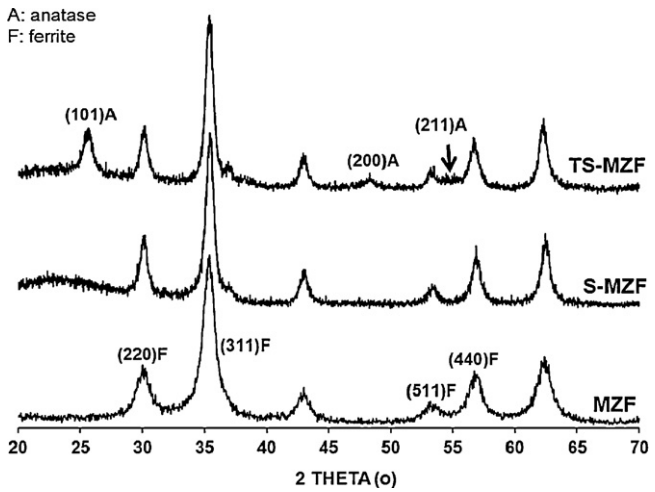

Fig. 7. X-Ray diffraction patterns of MZF, S-MZF, and TS-MZF (A = Anatase, F = Ferrite).

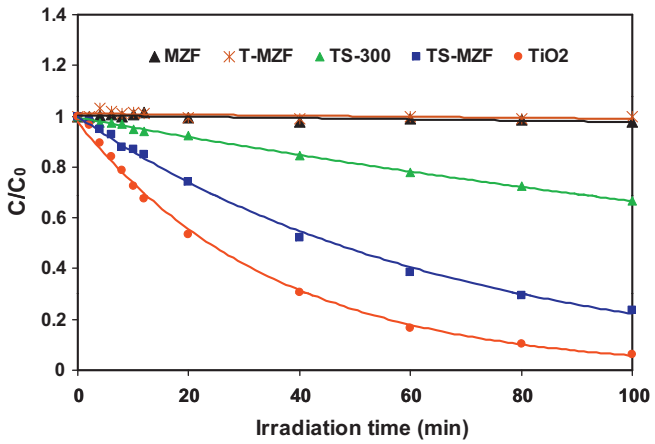

Fig. 9. Decomposition of methylene blue upon irradiation by the as-prepared catalysts.

decomposition appeared to be similarly unchanged in cases of MZF and T-MZF, demonstrating that neither was photoactive. To the best of our knowledge, this observation has never previously been reported. We learned from other literature [10,15,31,32] that the lack of an electron transferring inhibitor such as silica could only result in decreasing, but not completely suppressing, photoactivity. The reason for this observation possibly lies into two hypothetical causes. First, the MZF particle was completely encapsulated by the TiO_2 layer, which is consistent with the real core–shell structure suggested by Watson et al. [11] in that the charge transferred carriers are trapped inside the core, and thus cannot take part in the subsequent redox reaction with any reductant or oxidant in the solution. Second, the T-MZF was apparently formed with no phase separation after sintering. This two-materials merging negated their original properties and enhanced synergistic effect, which caused the reduction of photocatalytic and magnetic properties. Though this phenomenon was an important observation in the photocatalytic reaction of T-MZF, direct evidence to confirm the charge carrier transfer has not yet been observed. The preliminary study of photoluminescence (PL) to explore the role of silica as an inhibitor for electron transfer carried out in our laboratory was not successful. This might be due to the difficulty to observe radiation decay in TiO_2, which is an indirect-band gap semiconductor, at normal atmosphere [33]. A low-temperature study with time-resolved dynamic investigation [34] is necessary to acquire these data in further work.

Regardless, the influence of the interlayer thickness was also observed through the photocatalytic observation. The proper uses of TEOS volumes to form silica layers led to the formation of different thicknesses that influenced the reaction significantly. TS-MZF, obtained from 450 μL TEOS, displayed greater photocatalytic activity than that of TS-300 that was obtained from 300 μL TEOS. The thinner silica layer (Fig. 5) resulted in a decrease in photocatalytic performance. The selected amount of silica precursor was crucial; a small amount of TEOS may result in an incomplete silica coating, but excessive use can affect the magnetic property in the magnetic core. In our case, a silica thickness of 20 nm or so should be appropriate to pursue magnetic photocatalyst capability. Moreover, three recycled uses of a sample of TS-300 were carried out at room temperature to prove its stability. Fig. 10 reveals the performance of TS-MZF in removing MB without any decrease in photocatalytic activity.

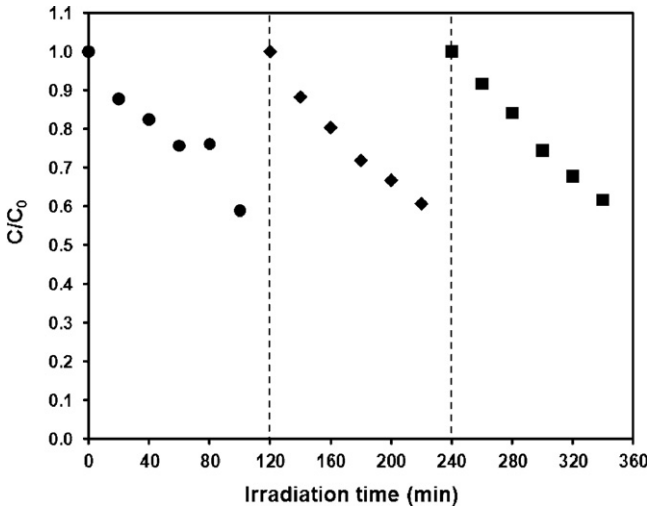

Fig. 10. Recycled photocatalytic decomposition of MB by TS-MZF.

4. Conclusions

The TiO_2/SiO_2/Mn–Zn ferrite composite was synthesized, and its properties were thoroughly investigated. With a simple co-precipitation method and no stabilizing agent, the three metal ion solutions were allowed to react with a base reagent to form magnetic nanoparticles. Suitable factors including rate of base addition and dispersion were used to synthesize nanoparticles of Mn–Zn ferrite with a superparamagnetic property. The hydrolysis of silica and titania precursors carried out stepwise led to the formation of magnetic photocatalyst TiO_2/SiO_2/Mn–Zn ferrite confirmed by several characterizations. The photocatalytic and magnetic properties were found to depend strongly on the semiconductor electronic interaction. It was observed that at least a minimum thickness of SiO_2 interlayer is required to prevent electron migration between the photocatalyst and magnetic core to maintain the photoactivity of the catalyst. Entirely photocatalytic suppression could be achieved when the interlayer silica was not introduced, suggesting the complete core–shell structure of titania/magnetic core.

Acknowledgements

This work was supported by the National Nanotechnology Center (Nanotec) with a grant funded by the National Science and Technology Development Agency (NSTDA); grant no. P-00-60061.

Appendix A. Supplementary data

Supplementary data associated with this article can be found, in the online version, at doi:10.1016/j.materresbull.2012.02.030.

References

[1] I.E. Wachs, in: J.L.G. Fierro (Ed.), Metal Oxides: Chemistry and Applications (Chemical Industries), CRC Press Taylor & Francis group, Boca Raton, 2006, pp. 2–4.
[2] M. Schiavello, A. Sclafani, in: N. Serpone, E. Pelizzetti (Eds.), Photocatalysis: Fundamentals and Applications, John Wiley & Sons, New York, 1989pp. 159–162.
[3] United States: Environmental Protection Agency, How to Evaluate Alternative Cleanup Technologies for Underground Storage Tank Sites, 2004 EPA 510-R-04-002, Chapter XIII, p.XIII-31-p.XIII-32.
[4] W. Wang, C.G. Silva, J.L. Faria, Appl. Catal., B 70 (2007) 470–478.
[5] H. Lorenz, J. Fritzsche, A. Das, K.W. Stöckelhuber, R. Jurk, G. Heinrich, M. Klüppel, Compos. Sci. Technol. 69 (2009) 2135–2143.
[6] G. Zhang, Express Polymer Lett. 5 (2011) 859–872.
[7] A. Goldman, Modern Ferrite Technology, Van Nostrand-Reinhold, 1990.
[8] J. Navio, G. Colon, M. Trillas, J. Peral, X. Domenech, J.J. Testa, J. Padron, D. Rodriguez, M.I. Litter, Appl. Catal., B 16 (1998) 187–196.
[9] D. Beydoun, R. Amal, G. Low, S. McEvoy, J. Mol. Catal. A: Chem. 180 (2002) 193–200.
[10] Y.S. Chung, S.B. Park, D.W. Kang, Mater. Chem. Phys. 86 (2004) 375–381.
[11] S. Watson, D. Beydoun, R. Amal, J. Photochem. Photobiol. A 148 (2002) 303–313.
[12] H.M. Xiao, X.M. Liu, S.Y. Fu, Compos. Sci. Technol. 66 (2006) 2003–2008.
[13] M.I. Litter, J.A. Navio, J. Photochem. Photobiol. A 84 (1994) 183–193.
[14] D. Beydoun, R. Amal, G.K.C. Low, S. McEvoy, J. Phys. Chem. B 104 (2000) 4387–4396.
[15] S. Xu, W. Shangguan, J. Yuan, M. Chen, J. Shi, Z. Jiang, Nanotechnology 19 (2008) 7, 095606.
[16] S.W. Lee, J. Drwiega, D. Mazyck, C.Y. Wu, W.M. Sigmund, Mater. Chem. Phys. 96 (2006) 483–488.
[17] X.F. Song, L. Gao, J. Am. Ceram. Soc. 90 (2007) 4015–4019.
[18] K. Mori, Y. Kondo, S. Morimoto, H. Yamashita, J. Phys. Chem. C 112 (2008) 397–404.
[19] C. Wang, L. Yin, L. Zhang, L. Kang, X. Wang, R. Gao, J. Phys. Chem. C 113 (2009) 4008–4011.
[20] M. Ma, Y. Zhang, X. Li, D. Fu, H. Zhang, N. Gu, Physicochem. Eng. Aspects 224 (2003) 207–212.
[21] V. Mohite, Self Controlled Magnetic Hyperthermia: Thesis, Florida State University, 2004, 21-22
[22] D. Makovec, A. Kosak, M. Drofenik, Nanotechnology 15 (2004) S160–S166.
[23] G. Schikorr, Z. Anorg, Allg. Chem. 212 (1933) 33–38.
[24] K. Parekh, R.V. Upadhyay, L. Belova, K.V. Rao, Nanotechnology 17 (2006) 5970–5975.

[25] H. Shunli, W. Xin, W. Yu, W. Yongming, L. Chunjing, Rare Met. 25 (2006) 466–470.
[26] D.K. Kim, Y. Zhang, W. Voit, K.V. Rao, M. Muhammed, J. Magn. Magn. Mater. 225 (2001) 30–36.
[27] M. Kimata, D. Nakagawa, M. Hasegawa, Powder Technol. 132 (2003) 112–118.
[28] W.L. Bragg, Proc. Cambridge Philos. Soc. 17 (1913) 43–57.
[29] K.T. Ranjit, B. Viswanthan, J. Photochem. Photobiol. A 108 (1997) 79–84.
[30] S. Rana, R.S. Srivastava, M.M. Sorensson, R.D.K. Misra, Mater. Sci. Eng. B 119 (2005) 144–151.
[31] S. Tawkaew, S. Supothina, Mater. Chem. Phys. 108 (2008) 147–153.
[32] H. Zhang, R. Hou, Z.-L. Lu, X. Duan, Mater. Res. Bull. 44 (2009) 2000–2008.
[33] Y. Li, C. Song, Y. Wang, Y. Wei, Y. Wei, Y. Wei, Y. Hu, Luminescence 22 (2007) 540–545.
[34] V. Melnyk, V. Shymanovska, G. Puchkovska, T. Bezrodna, G. Klishevich, J. Mol. Struct. 744–747 (2005) 573–576.